Chapter 7

Internal Electrode Motion

Preliminary animal reconstructions have been presented in part at: the 21st International Conference on Biomedical Applications of Electrical Impedance Tomography (EIT 2021) (Stowe et al.*, 2021).*

7.1 Introduction

As discussed in section 2.2, several factors contribute towards the cardiosynchronous signal in EIT. One of the largest contributions is movement; both the movement of body structures and the movement of electrodes contribute significantly to the measured impedance and the resulting reconstructed image (Adler *et al.*, 2017b; Proença *et al.*, 2015). The previous chapters support that more accurate meshing and internal electrodes may help to identify the movement of structures and organs, isolating their impact on the reconstructed images, but the problem of electrode motion is amplified when internal electrodes are used. Internal electrodes placed

on a probe are challenging to locate within a subject due to variation in individual geometries. Incorrectly modelling the electrode locations can introduce an artefact in the image (Boyle and Adler, 2011), but in time difference EIT these effects are minimized (Adler and Boyle, 2017). The larger problem appears to be the movement of the internal probe relative to the external electrodes between measurements.

Movement correction algorithms using the movement jacobian have been designed in 2D and 3D (Gómez-Laberge and Adler, 2007; Gómez-Laberge and Adler, 2008; Soleimani *et al.*, 2006) and used to reconstruct electrode movement on 3D models with a 2D arrangement of electrodes (Boyle, 2016). There are several available methods to calculate the movement jacobian (Boyle *et al.*, 2017), the simplest of which, the naïve perturbation method (Gómez-Laberge and Adler, 2008), has been used in this chapter as a proof of concept. A more detailed explanation of this jacobian calculation method is presented in section 2.4.6.1 of the background. As an internal probe moves towards one side of a model the distance between the probe and the external electrodes changes. This results in less impedance where the distance has decreased, and a higher impedance where the distance has increased. Without knowing the new probe location we can minimize the effect of this error, but there still remains a mismatch between the modelled and actual probe locations. The artefact that is reconstructed can give hints regarding the motion of electrodes, although it can be difficult to separate the effect of electrode movement from biological impedance changes of interest (Boyle, 2016).

This chapter presents a method that builds on current algorithms available, to create a new, corrected model that helps to compensate for the effect of electrode

movement. The known shape of the artefact due to movement of the probe is used to derive the probe location, and create a corrected model to improve reconstruction accuracy in the presence of probe motion.

The goal of this chapter is to establish a technique to reduce the impact of probe movement on image reconstructions, and then to use this technique in an animal model. Although simulations in 2D and now in 3D show that internal electrodes can provide a desirable increase in sensitivity, the benefit has not been realized in real-world recordings. This chapter presents a novel method to correct for electrode displacement artefacts, and compares established techniques for 3D EIT image reconstruction to reconstructions with the novel internal electrode approach in a limited number of subjects.

7.2 Methods

This chapter consists of two experiments: a simulation study correcting for probe motion in a tank model, and preliminary *in-vivo* recordings that were conducted as an addition to another experimental protocol.

7.2.1 Simulations

Simulations were done using EIDORS (v3.10) (Adler *et al.*, 2017a) using Matlab 2019b (Matworks, Natick, MA, USA). Within EIDORS, meshes were generated using Netgen (version 5.3.1) (Schöberl, 1997).

7.2.1.1 Tank models

A model of a tank with 28 external electrodes placed in two planes of 14 evenly around the exterior and 4 internal electrodes was created. The tank radius and height were 1 m, and the external electrode radius was 5 cm. The external electrode planes were placed at a height of 0.3 m and 0.7 m on the tank. The internal electrodes were spaced evenly between the external electrode planes at 0.3 m, 0.433 m, 0.567 m and 0.7 m. The internal electrodes were specified in two different ways. The first used spheres with a radius of 2.5 cm, and the second used a hollow cylinder with a radius of 2.5 cm containing cylindrical electrodes with a radius of 2.5 cm and a height of 5 cm. External electrodes were placed in a "square" electrode configuration (Grychtol *et al.*, 2016). Both models are shown in figure 7.1.

These models were compared to confirm that both performed adequately with motion correction, as internal electrodes are challenging to model and many different techniques are used. When using internal electrodes on a complex model, it is currently easiest to add electrodes along a hollow tube cut through the centre.

To specify a conductive region elements within a radius were assigned a conductivity of twice the background conductivity of the tank model. The conductive target was placed midway between the centre of the tank and the boundary. The radius of the target was 20 cm. Figure 7.1 shows the conductive target for both internal probe types.

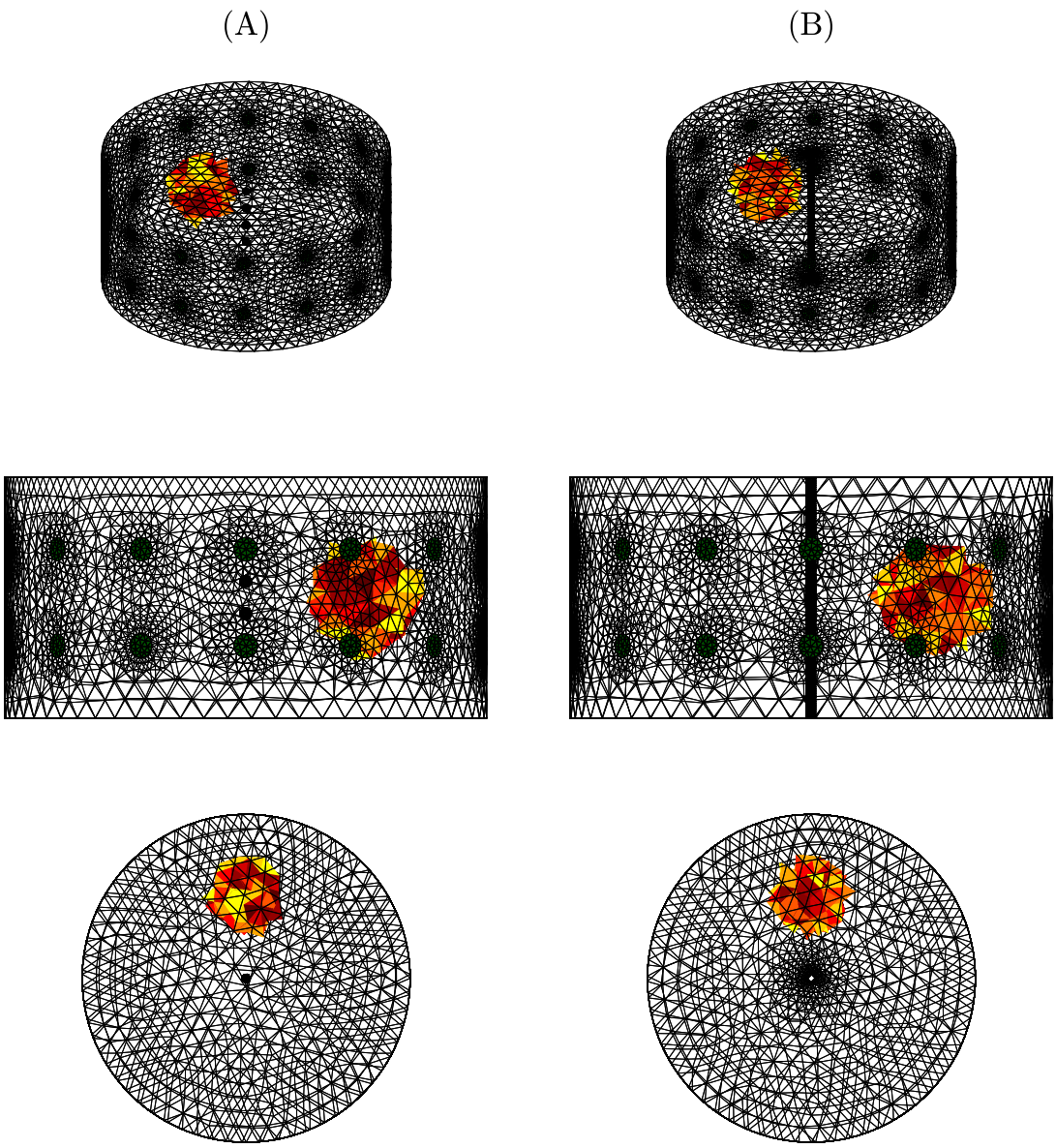

Figure 7.1: On the left (A) internal electrodes were modelled as 4 spherical electrodes between the external electrode planes. On the right (B) the internal electrodes were created using a hole through the centre of the model and using cylindrical electrodes on the inner surface of the model. The conductive region was specified by setting the conductivity of all elements contained in the target to be twice the background conductivity.

7.2.1.2 Measurements

Despite sensitivity advantages ascribed to custom injection and measurement patterns, the skip 4 pattern was used as it is straight forward to implement with currently available EIT systems.

Reference measurements were made with no conductive object and electrodes in the centre of the model. Measurements with a conductive object were made with the probe centred, then with the probe was shifted by 1, 5, and 10 percent of the tank radius in a randomized direction. The direction was randomized between trials but was consistent for each of the 1, 5 and 10 percent probe error models that were compared.

7.2.2 Movement correction

The movement correction jacobian was calculated using the methods presented by Gómez-Laberge and Adler (2008). In a model with a centred electrode probe and uniform conductivity, each of the four electrodes on the probe was perturbed by 0.001 m in each of the **x**, **y**, and **z** directions. A measurement was made for each electrode and each of the three dimensions of movement. The resulting measurements were divided by the perturbation amount. The measurements on each electrode (V_j) and from each direction of movement (**x**, **y**, and **z**) were combined to form the movement jacobian (J_M) using the following equation from Gómez-Laberge and Adler (2008):

$$J_M = \left[\frac{\partial \mathbf{V}_j}{\partial \mathbf{x}}, \frac{\partial \mathbf{V}_j}{\partial \mathbf{y}}, \frac{\partial \mathbf{V}_j}{\partial \mathbf{z}} \ldots \frac{\partial \mathbf{V}_n}{\partial \mathbf{x}}, \frac{\partial \mathbf{V}_n}{\partial \mathbf{y}}, \frac{\partial \mathbf{V}_n}{\partial \mathbf{z}} \right] \tag{7.1}$$

This movement jacobian was used in conjunction with the following single-step formulation for a reconstruction matrix presented by Adler *et al.* (1994). The regular impedance based reconstruction matrix is denoted by R_C and the jacobian for impedance based reconstruction is denoted by J_C.

$$R_C = \frac{[J_C]^T[W]}{[J_C][W][J_C]^T + [W]} \tag{7.2}$$

W in the above equation represents the Laplace prior (Soleimani *et al.*, 2006). Combining this formulation with the movement jacobian yields the following equation for the reconstruction matrix (R_M) (Soleimani *et al.*, 2006) where R_M denotes the reconstruction matrix for motion correction.

$$R_M = \frac{[J_C]^T[W]}{[J_C][W][J_C]^T + \mu[J_M][J_M]^T + [W]} \tag{7.3}$$

In the above equation μ represents the weighting of the motion correction. In this experiment the motion correction weighting was set to 100.

Combining equation (7.2) and equation (7.3) a reconstruction matrix to reconstruct exclusively the noise due to movement (R_N) in an image can be generated.

$$R_N = R_M - R_C \tag{7.4}$$

An image (X) is reconstructed using the measurements (b) and reconstruction matrix (R) as follows:

$$X = bR \tag{7.5}$$

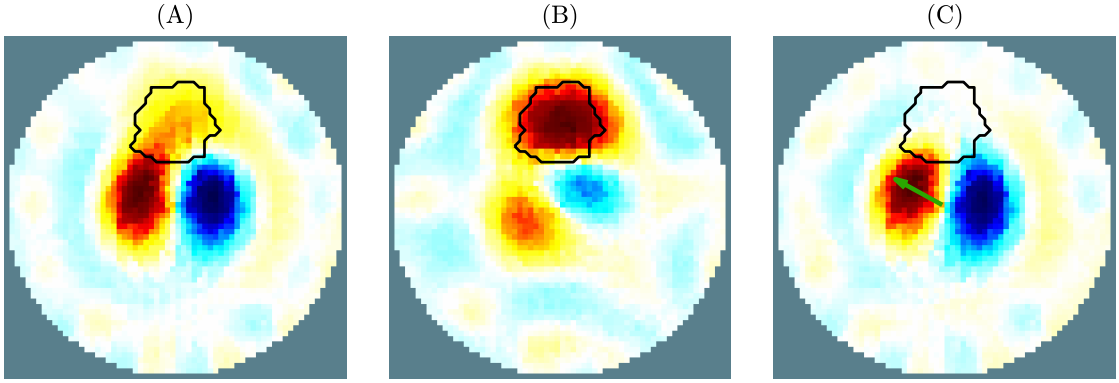

Figure 7.2: Three image reconstruction matrices were generated: one to calculate an image based only on the measurements (A), one that is able to reduce the impact of noise using a movement jacobian (B) and finally a reconstruction that reconstructs only the noise due to motion of the probe (C). The centre of mass of the conductive object is used to estimate the probe location and direction of movement. The green arrow indicates the calculated direction of movement (multiplied by 5 for visibility). The black line indicates the outline of the region of conductivity at the imaged plane. The images depict an average of 10 slices between the external electrode planes.

Three images: X_C, X_M and X_N were reconstructed from their respective reconstruction matrix.

A new movement correction strategy had been built around the reconstructed image X_N. The noise due to exclusively motion is reconstructed into a 3D image, and the centre of mass of the positive change is located. This is assumed to be the direction of the motion. The amplitude of the electrode motion is estimated as half of the distance between the conductive artefact and the probe. This method is illustrated in figure 7.2. Images were reconstructed and displayed on a 64 by 64 grid to give a more accurate representation of the electrode position in the reconstructed image.

Using the probe location estimate calculated from X_N a new model was reconstructed with the probe repositioned to the reconstructed location. This model was

then used to calculate a new reconstruction matrix using equation (7.3) with an updated jacobian based on the new probe location.

7.2.3 Image comparison

To simplify processing of the reconstructions, 10 images between the external electrode planes were averaged together to generate a 2D representation of the 3D data. This did not allow for analysis of movement in the vertical direction, but we did not expect this to be a major contribution in real-world data. The reconstructed images were compared in two ways. First the accuracy of the reconstruction was evaluated by computing the Jaccard index between the actual and imaged boundaries of the conductive target. The imaged boundary was drawn at half the maximum value of the brightest object in the image. The second metric computed was a noise estimate. This was calculated as the amplitude of the imaged object relative to the amplitude of the entire image through the following equation:

$$N = 1 - \frac{A_{\text{object}}}{A_{\text{image}}} \tag{7.6}$$

Where A_{object} is the amplitude of the object, A_{image} is the amplitude of the image, and it is subtracted from 1 so that a noise estimate of 0 corresponds with all of the image signal corresponding to the conductive target.

7.2.4 *In-vivo* recordings

Data were collected in three ewes during ventilation under general anesthetic using the SenTec EIT Pioneer Set. A skip 4 measurement pattern was used with an injection current of 3 mA at 30 kHz. Electrodes 29 to 32 were connected to the internal electrode probe.

7.2.4.1 Internal electrode probe design

The internal electrode probe consisted of four brass electrodes on a flexible tube. Each electrode was 1 cm in length and the spacing between electrodes was 2 cm. The electrodes were created from a brass sheet with a thickness of 2 mm that was bent to the shape of the flexible tubing and soldered to achieve a smooth surface. The electrodes were glued in place on the tube protruding 2 mm from probe surface. The tube radius was 0.5 cm. The constructed probe is shown in figure 7.3.

7.2.4.2 Electrode placment

The ewes were shaved and silver-silver chloride electrodes were placed in 2 rows immedeately behind the front legs with 10 cm seperation. The esophageal probe was allighed with the electrodes externally and the required depth was marked. The electrode probe was then coated in a conductive gel for lubraction and inserted in the esophagus up to the marked point.

Figure 7.3: A prototype of an internal electrode probe for esophageal use in an ovine model. Four brass electrodes are bent around the outside of a flexible tube designed for esophageal use. Edges of the electrodes are soldered and filed to be smooth. The electrodes are glued in place and wires run down the hollow centre of the tube to connect to the EIT system.

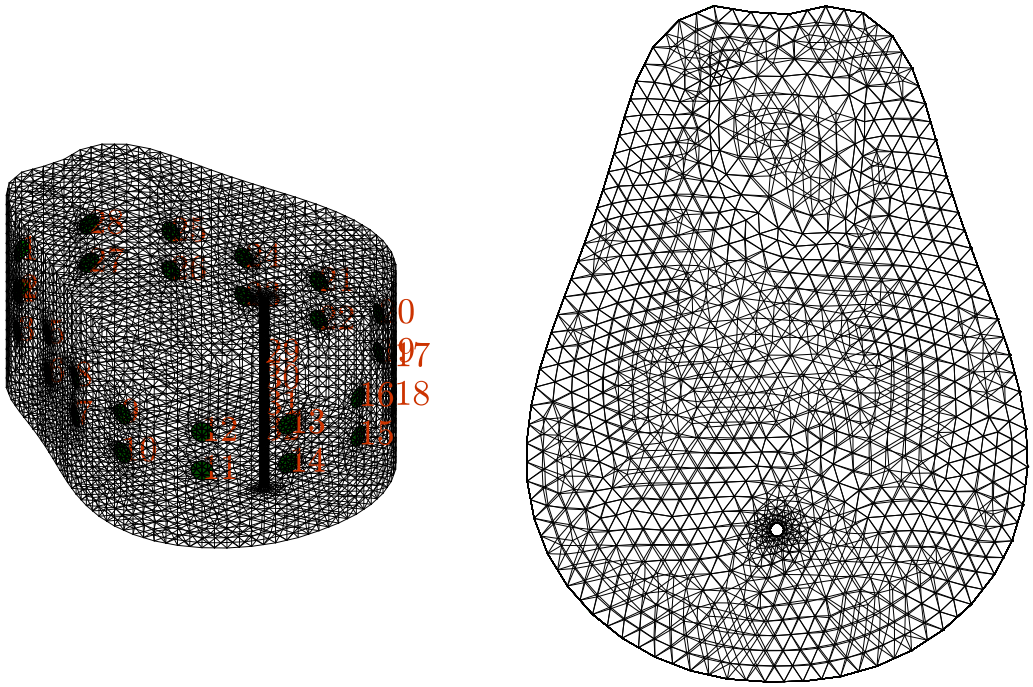

Figure 7.4: An internal electrode was added to an ovine model by creating a hole at desired probe location and added cylindrical electrodes at the desired heights. External electrodes were placed in a "square" electrode configuration on the boundary. Electrodes 1 to 28 were external and 29 to 32 were internal.

7.2.4.3 Ovine model

An internal probe was added to an ovine model by adapting the `mk_library_model` function in EIDORS (Adler *et al.*, 2017a). A circular region was added to the library geometry, and was extruded upwards to make a hole at the probe location. External electrodes were placed in a square pattern on the boundary, and internal electrodes were added as cylindrical objects in the central hole of the model. The resulting model is shown in figure 7.4.

7.2.4.4 Reconstruction

Images were reconstruted with 4 methods. The 3 methods discussed in section 7.2.2, and GREIT (Grychtol *et al.*, 2016).

7.2.4.5 Pulsatile amplitude

To measure the advantage provided by internal electrodes with regard to cardiosynchronous signal detection, a fast Fourier transform (FFT) of each signal was calculated. The cardiosynchronous component was selected as the highest amplitude near the recorded heart rate range of 65–80 bpm. This was divided by the amplitude of the ventilation frequency, which was the largest low-frequency amplitude in the FFT of the detrended signal. This was repeated for all 12 recordings across 3 animals.

7.3 Results

The following section presents the results for both simulation and *in-vivo* work.

7.3.1 Simulation

It was found that there was no measurable difference between simulations of models using spherical internal electrodes relative to the cylindrical electrodes. The results are presented using the cylindrical model to be consistent with the lamb models. The probe was moved in in the $-\mathbf{y}$ direction for figures and calculations in the results.

Figure 7.5 shows the result of the three reconstruction methods. The boundaries of the reconstructed and actual targets are outlined to highlight the performance.

Table 7.1: The jaccard index was calculated for each of the reconstructions in figure 7.5. Method A does not use any motion correction. Method B incorporates the movement jacobian, and method C uses the new probe location correction technique. For jaccard index, a score closer to one is better.

Movement (% of radius)	Method A	Method B	Method C
1	0.732	0.809	0.802
5	0.038	0.654	0.808
10	0.003	0.227	0.577

Table 7.2: Noise estimate values calculated for each of the reconstructions in figure 7.5. Method A does not use any motion correction. Method B incorporates the movement jacobian, and method C uses the new probe location correction technique. For the noise estimates a lower score is better, a score of zero indicates all image changes occur within the target boundary, and a score less than one indicates most of the changes in the image are due to the identified target.

Movement (% of radius)	Method A	Method B	Method C
1	0.588	0.537	0.529
5	0.781	0.669	0.618
10	0.777	0.747	0.718

The new method is able to reconstruct the correct location with motion of up to 10 % of the tank boundary between measurements. The jaccard index and noise estimate for each method are presented below in table 7.1 and table 7.2.

For movement of one percent of the tank boundary motion correction using only the movement jacobian was roughly equivalent to the probe location correction algorithm. Across all other scenarios, the probe location correction algorithm achieved a higher jaccard score. Across all scenarios the new technique to correct for motion had the lowest noise estimate score.

When looking at the reconstructions using the three methods, the new probe correction technique reconstructed the target as the brightest object in all scenarios. With no motion correction, the target was identified correctly only in the first

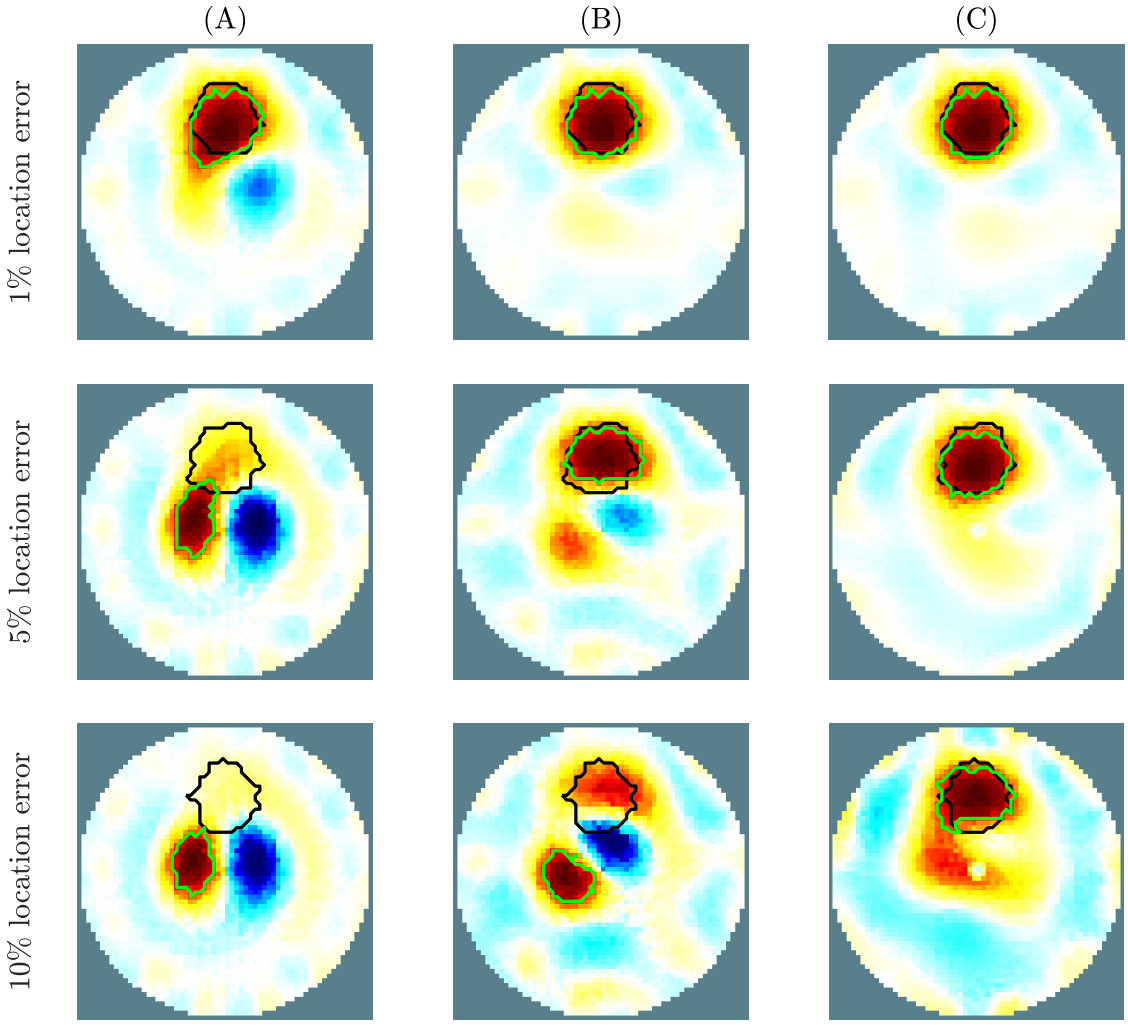

Figure 7.5: The results of the probe location correction are presented. The rows from top to bottom show results with 1, 5, and 10% shifts in probe location relative to the tank radius. Column (A) shows the results of the reconstruction with no motion correction, column (B) shows the method using the movement jacobian, and column (C) shows the results of the new probe location correction method. The green outline indicates the reconstructed boundary of the conductive target, and the black outline is the actual boundary.

scenario. Using the movement jacobaian reconstruction method, the target was correctly identified when the probe was moved one or five percent of the tank radius.

7.3.2 *In-vivo*

Recordings in each of the three ewes are presented in this section. Reconstructions with internal electrodes are shown in figure 7.6 for a selected breath during a baseline recording in each subject.

Reconstructions with movement correction applied to the internal electrodes appear to show a slight improvement in lung distinguishability and a slight reduction in noise surrounding the probe. There is limited difference between the two methods accounting for motion on the electrode.

The ratio of cardiosynchronous to respiratory rate impedance signals is shown below in figure 7.7. The results show a higher amplitude of the cardiopulmonary signal relative to ventilation when internal electrodes are used.

7.4 Discussion

This chapter aimed to provide a technique to reduce noise due to motion on internal electrodes when reconstructing images in 3D and demonstrate the noise reduction technique *in-vivo*. The new technique to reconstruct images in the presence of motion on internal electrodes reconstructed an image of a conductive target more accurately and with less noise in the surrounding image. *In-vivo* reconstructions

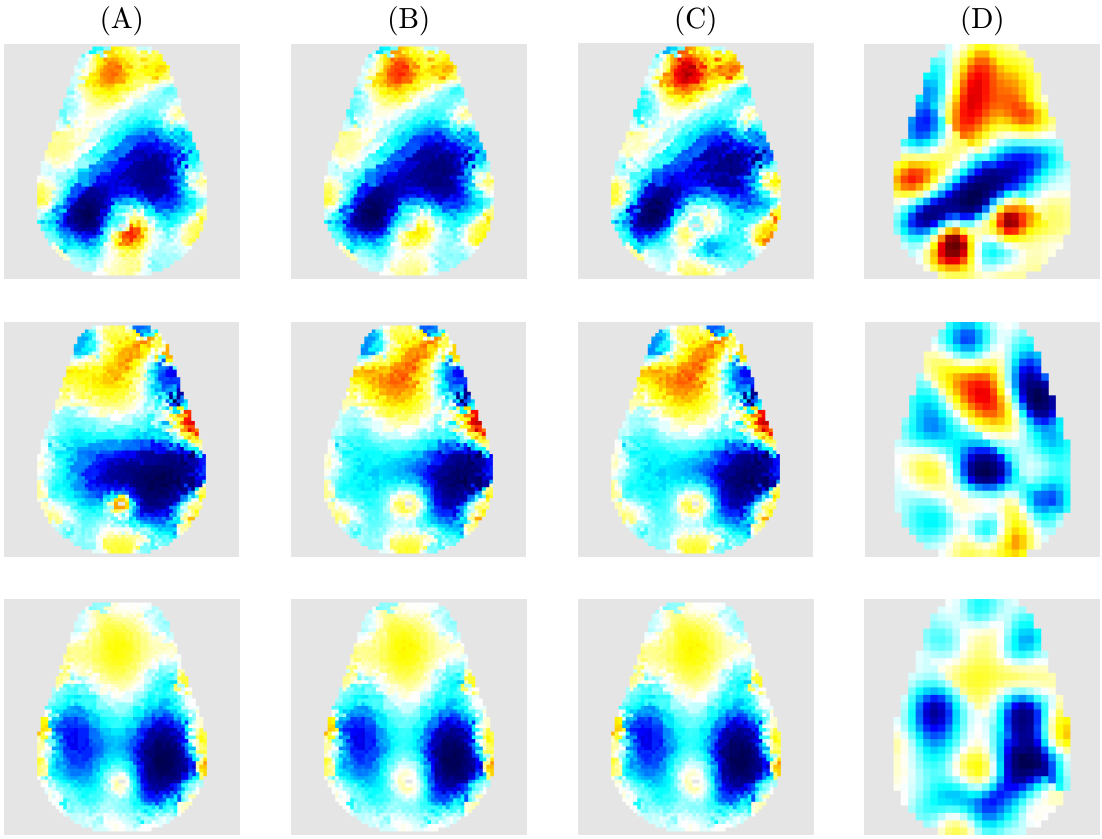

Figure 7.6: Preliminary results on 3 ewes reconstructed from a single, selected breath. Each column represents a reconstruction method. Column (A) uses no motion correction, column (B) uses the movement jacobian and column (C) uses the new method for electrode location correction. Column (D) contains reconstructions using the GREIT 3D algorithm. The number of pixels is different between images due to the methodology of probe localization and the limitations of GREIT.

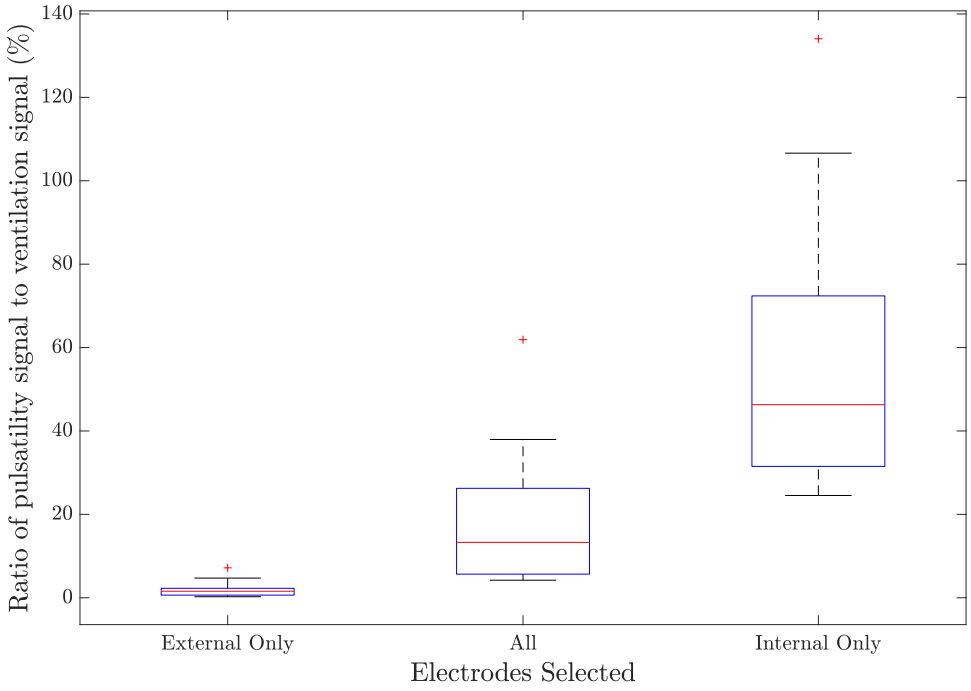

Figure 7.7: The cardiosynchronous signal component was divided by the ventilation frequency componenent to compare the detectability of the pulsatile changes. The ratio was compared for measuremnts using only external electrodes, all electrodes, and internal electrodes only.

showed a slight improvement in lung distinguishability when correcting for motion artefacts on internal electrodes compared to methods without this correction including GREIT. Results in 3D also confirmed results from a 2D study in a porcine model showing an increased cardiosynchronous component on the internal electrode measurements (Czaplik *et al.*, 2014).

It was found that GREIT performed poorly when reconstructing data with internal electrodes. The figures of merit for GREIT designed and optimized to work with external electrodes where sensitivity is low in the centre of the model and high at the edges (Adler *et al.*, 2009). An adaptation to GREIT that is able to account for internal electrodes and motion of an internal probe is planned as a continuation of this project.

Two types of internal electrodes were modelled in this chapter. One with spherical internal electrodes and one with a hollow probe and cylindrical electrodes. Meshing and creating internal electrodes can be challenging due to limited meshing tools for using internal electrodes with EIT and the method of adding internal probes to anatomical models using a hollow region in the centre of the model was created for this project. Code to generate this model with internal electrodes is planned to be included in a future release of EIDORS.

The noise estimate score calculations were not perfect representations of the noise in the images due to the way the reconstructed object was identified. Since the brightest object was always identified as the object, the noise estimate was artificially low in some cases. Comparing the amplitude of changes contained within the true object boundaries could be a better metric of the noise present in the image, but this

would also be dependent on the accuracy of reconstruction and would have favoured the method that reconstructed the object most accurately. The boundary of the true target also changes due to differences in element locations as the probe is moved, so the comparison would not be consistent across all probe movement states. Despite this limitation, the noise estimate does help to quantify noise seen in the images for each technique. The new method performed better than existing techniques across all situations according to the computed noise metrics.

In simulated cases of less than one percent error in probe location, very little difference in reconstruction accuracy between the two motion correction algorithms was detected. Despite this, a slight reduction in background noise in the image was observed.

Despite the improvements to reconstruction accuracy and noise reduction using the new method, there are several limitations to its use. The most significant is the increased modelling time required. This method required an extra model, and inverse solution compared to the single step solutions. For simple models such as a tank the added time difference is small, but for complex models this could increase reconstruction time drastically. When several frames are reconstructed each requires a unique model with a modified probe location increasing the time required significantly. To reduce the reconstruction time, correcting the model only when the probe location error is greater than one percent of the model radius may be helpful. At this level of movement, the benefits of the probe localization technique are not substantial. Additionally in the images presented probe movment did not appear to be significant. It is not yet clear what the typical movement of the electrode probe

is expected to be in the esophagus.

Previous research has also reconstructed for motion direction directly using the movement jacobian (Boyle, 2016; Gómez-Laberge and Adler, 2008; Soleimani *et al.*, 2006). This technique for electrode estimation has not been implemented using internal electrodes for this research, but a comparison between the two electrode position estimation techniques it required for complete validation of the demonstrated method.

Previous studies with internal electrodes showed cases where contact impedance of the probe was inadequate for electrodes placed on the breathing and feeding tubes (Czaplik *et al.*, 2014). The electrodes used were shown to have a good contact impedance on the SenTec Pioneer Set interface, but the current design protrudes slightly from the tube and may be challenging to integrate into a clinical esophageal or tracheal tube.

Sanchez *et al.* (2013) used an array of internal electrodes in the lung during biopsy procedures, and suggested that the increased proximity to the tissue could allow more physiological information to be obtained. A more complete evaluation is required to measure the benefits of internal electrodes in 3D compared to typical external configurations. The previously seen lung distinguishability and larger cardiosynchronous signal amplitude found in 2D(Czaplik *et al.*, 2014) have been repeated with this 3D configuration, but it is still unclear to what degree these signal changes may be useful.

Increased lung separability may be useful for determining the difference between right and left lung ventilation, which can be used to quantify ventilation perfor-

mance (Sage *et al.*, 2018) and is an important step in detecting ventilation and perfusion mismatch (Kircher *et al.*, 2021; Leonhardt and Lachmann, 2012; Stowe *et al.*, 2019). Increased sensitivity to pulsatile flow may also help to improve measures of cardiopulmonary activity where detecting pulsatile flow and motion in specific regions of a model is desired (Braun *et al.*, 2018; Proença *et al.*, 2020).

7.5 Summary

Probe displacement introduces significant errors when using reconstruction algorithms that do not account for movement. This chapter presents a new technique designed to reduce the effect of probe motion. This new method was found to outperform existing methods with regards to reconstruction accuracy and background noise in simulations on a tank model. Internal electrodes in conjunction with a 3D external configuration were also used *in-vivo* to measure ventilation. Images of breaths across three subjects showed an improvement to lung distinguishability when correcting for motion, and the average ratio of cardiosynchronous to pulmonary signal was increased when using internal electrodes.